Sentinels4Carbon (Sense4Fire)

Sentinel-based fuel, fire and emissions products to constrain the changing role of vegetation fires in the global carbon cycle

ESA Contract Number: 4000134840/21/I-NB

Database Description

7th November 2021, Version 1

Prepared by:

Matthias Forkel, Christine Wessollek, Christopher Marrs

Technische Universität Dresden, Faculty of Environmental Science, Dresden, Germany

Vincent Huijnen, Jos de Laat, Martin de Graaf

Royal Netherlands Meteorological Institute (KNMI), De Bilt, The Netherlands

Niels Andela, Alfred Awotwi

Cardiff University, School of Earth and Environmental Sciences, Cardiff, Wales, UK

Contents

1 Overview of datasets

The datasets as listed in Table 1 will be used as input data in Sense4Fire. The data is collected at a shared network drive hosted at TU Dresden. All partners have access to the network drive.

Table 1: Overview of input datasets for Sense4Fire.

Dataset (Sensor)	Variables	Spatial resolution and coverage	Temporal resolution and coverage	WP	URL / DOI or reference
Sentinel-3/OLCI and Proba-V	FAPAR, fCOVER, LAI	300 m, global	3 days, since 2014	WP 3, WP 4	https://land.copernicus.eu/global/products/fapar, https://land.copernicus.eu/global/products/fcover, https://land.copernicus.eu/global/products/lai
Sentinel-3/OLCI+SLSTR L2-SYN	Surface reflectance	300 m, global	3 days, since 2016	WP 3, WP 4	https://sentinel.esa.int/web/sentinel/user-guides/sentinel-3-synergy
Sentinel-2	Surface reflectance	20 m, (regional)	Large number of fires for cal./val.	WP 3, WP 4	https://sentinel.esa.int/web/sentinel/user-guides/sentinel-2-msi
Sentinel-1	Surface soil moisture	1 km, global	since 2015	WP 3, WP 4	https://land.copernicus.eu/global/products/ssm
Soil moisture_cci	Surface soil moisture	0.25°, global	daily, 1978-2019	WP 3, WP 4	https://www.esa-soilmoisture-cci.org/
Metop-ASCAT	Soil water index (SWI)	0.1°, global	daily, since 2007	WP 3, WP 4	https://land.copernicus.eu/global/products/swi

Biomass_cci	Above-ground biomass (forests)	100 m, global	2010, 2017, 2018	WP 3, WP 4	http://dx.doi.org/10.5285/bedc59f37c9545c981a839eb552e4084
Global Forest Canopy Height	Forest Canopy Height	30 m, global (52°N-52°S)	2019	WP 3, WP 4	https://glad.umd.edu/dataset/gedi
Land cover_cci	Land cover	300 m, global 20 m, Africa	annual, 1992-2015 (2016)	WP 3, WP 4	https://climate.esa.int/en/projects/land-cover/data/#mrlc-maps-v207 https://cds.climate.copernicus.eu/cdsapp#!/dataset/satellite-land-cover
Global fuelbed map	Fuelbed classification, fuel loads	polygons, global	approximately representative for 2010	WP 3, WP 4	https://doi.pangaea.de/10.1594/PANGAEA.849808
NAWFD	Fuelbed classification, fuel loads			WP 3, WP 4	https://fuels.mtri.org
BAAD	Tree allometry, biomass in tree components			WP 3, WP 4	https://doi.org/10.6084/m9.figshare.c.3307692.v1
VODCA VOD	Vegetation Optical Depth	0.25°, global	daily, 1987-2018 (depending on band)	WP 3, WP 4	https://zenodo.org/record/2575599

SMOS-IC VOD	Vegetation Optical Depth	0.25°, global	3 days, since 2009	WP 3, WP 4	https://www.theia-land.fr/en/product/smos/
MODIS	Life fuel moisture content	500 m, global	8 days, since 2000	WP 3, WP 4	(Yebra et al., 2018)
PRODES Historic deforestation rates	Fire classification	30 m, Brazil	annual	WP 3, WP 4	https://data.globalforestwatch.org/datasets/prodes-deforestation
Hansen forest loss	Forest cover/loss	30 m, global	annual	WP 3, WP 4	(Hansen et al., 2013)
High latitude peatland extent and carbon	Fire classification	10 km, northern hemisphere high latitudes	recent	WP 3, WP 4	(Hugelius et al., 2020)
Sentinel-3 SLSTR active fire detections, FRP	Fire perimeter, speed, duration.	1 km, global	2 times daily (10 am/pm)	WP 3, WP 4	(Weidong et al., 2020)
NOAA20/S-NPP VIIRS active fire detections, frp	Fire type (persistence, intensity, diurnal cycle)	375 m global	2 times daily (1:30 am/pm)	WP 3, WP 4	(Schroeder et al., 2014)
Sentinel-2 Fire cci burned area	Burned area associate with	20 m, Africa	2016	WP 3, WP 4	(Roteta et al., 2019)

	fire perimeters and small fire thermal anomalies				
L2_CO (Sentinel-5p)	CO total column		daily	WP 3, WP 4	https://doi.org/10.5270/S5P-bj3nry0 https://doi.org/10.5270/S5P-1hkp7rp
L2_NO2 (Sentinel-5p)	NO2 tropospheric column	5.5×3.5 km²	daily	WP 3, WP 4	https://doi.org/10.5270/S5P-9bnp8q8 https://doi.org/10.5270/S5P-s4ljg54
L2_HCHO (Sentinel-5p)	HCHO tropospheric columns	5.5×3.5 km²	daily	WP 3, WP 4	https://doi.org/10.5270/S5P-vg1i7t0 https://doi.org/10.5270/S5P-tjlxfd2
L2_AER_AI (Sentinel-5p)	Aerosol index	5.5×3.5 km²	daily	WP 3, WP 4	https://doi.org/10.5270/S5P-3dgz66p https://doi.org/10.5270/S5P-0wafvaf
L2_AER_ALH (Sentinel-5p)	Aerosol Layer Height	5.5×3.5 km²	daily	WP 3, WP 4	https://doi.org/10.5270/S5P-7g4iapn https://doi.org/10.5270/S5P-j7aj4gr
GFAS	Trace gas and aerosol fire emissions	50×50 km²	daily (hourly)	WP 3, WP 4	https://atmosphere.copernicus.eu/global-fire-emissions
GFED	Trace gas and aerosol fire emissions	0.25 degree	since 1997, monthly (daily and 3-hourly scaling available)	WP 3, WP 4	https://globalfiredata.org/pages/data/ (van der Werf et al., 2017)

2 Datasets for surface and fuel conditions

2.1 Sentinel-3/OLCI and Proba-V FAPAR/LAI/fCOVER

The Ocean and Land Colour Instrument (OLCI) onboard Sentinel-3 is a medium-resolution multi-spectral instrument. It allows the mapping of land cover conditions in the visible and near-infrared domain at medium spatial resolution (300 m). The Proba-V satellite was designed to bridge between the end of SPOT-5 VGT observations and the advent of Sentinel-3A. The Proba-V instrument provides observations in the visible and near infrared at a spatial resolution of 333 m.

Observations from OLCI and Proba-V are used to retrieve vegetation properties such as the fraction of absorbed photosynthetic active radiation (FAPAR, the OLCI Global Vegetation Index), leaf area index (LAI) and the fraction of green vegetation cove (fCOVER) at a resolution of 333 m. The product has been available since January 2014 as near-real time 10-daily product. Version 1.0 of the algorithm uses Proba-V observations s input, version 1.1 uses Sentinel-3/OLCI observations. The estimation of the biophysical parameters is performed using neural networks. The production of FAPAR, LAI, fCOVER estimates includes a temporal smoothing and gap filling to reduce noise in time series. Observations from several days are combined in a 10-daily near-real time estimate. This estimate is then changed to a consolidated value after two months of observations (https://land.copernicus.eu/global/sites/cgls.vito.be/files/products/CGLOPS1_ATBD_FAPAR300m-V1.1_I1.02.pdf). The combined Sentinel-3/OLCI and Proba-V FAPAR product as well as LAI and fCOVER are available from the Copernicus Global Land Service: https://land.copernicus.eu/global/products/fapar.

The FAPAR, LAI and fCOVER products will be used as input into the approach to estimate the temporal dynamic of canopy and herbaceous fuel loads. Furthermore, the FAPAR product will be also used as one input to a machine learning model to estimate the fuel moisture content of living grass and leaves in canopies (LFMC).

2.2 Sentinel-3/OLCI+SLSTR L2-SYN

The combination of the OLCI and the SLSTR (Sea and Land Surface Temperature Radiometer) sensors from Sentinel-3 allow to retrieve land surface reflectance and aerosol parameters in continuation of the SPOT VGT instrument (https://sentinels.copernicus.eu/documents/247904/349589/SYN_L2-3_ATBD.pdf). These so called SYN products have a spatial resolution of 300 m and cover various bands from the visible to the short wave infrared (Figure 1). The SYN products provide measurements of both instruments on the OLCI image grid.

The Sentinel-3 SYN surface reflectance bands will be specifically useful to estimate live-fuel moisture content (LFMC). Especially spectral bands along the red edge (Oa10 to Oa14) and in the short-wave infrared (S5 and S6) should be mainly sensitive to estimate LFMC. Therefore Sentinel-3 bands will be calibrated against a global database of LFMC measurements (Yebra et al., 2019).

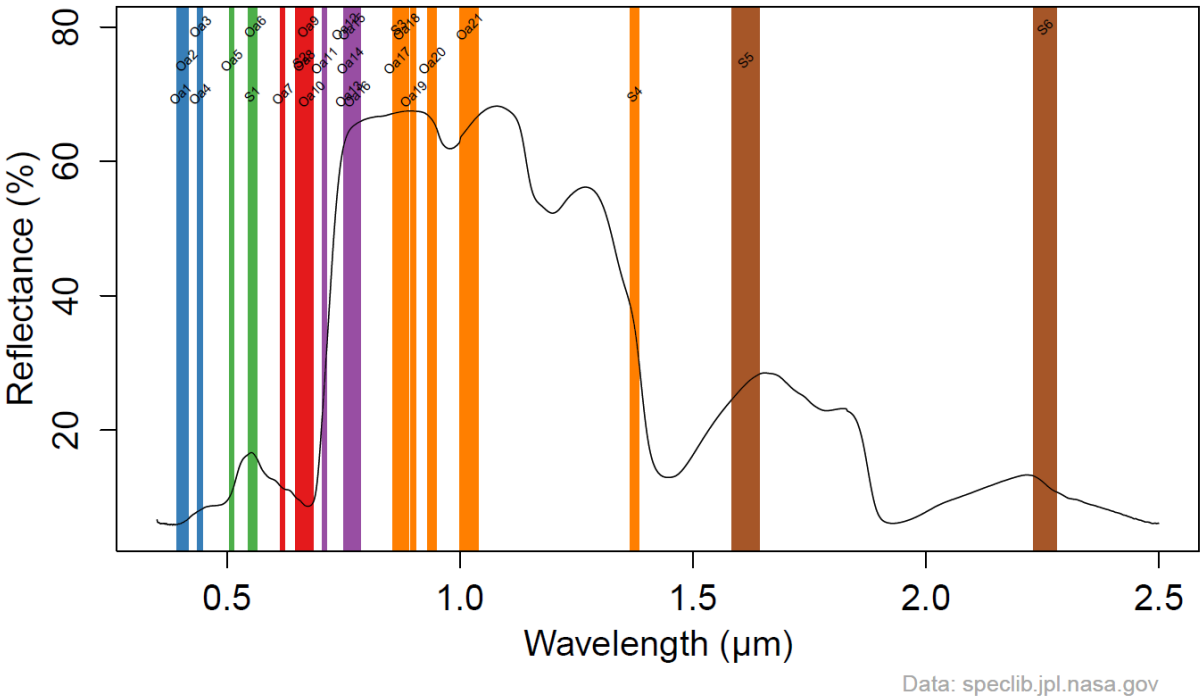

Figure 1: Location of the Sentinel-3 OLCI and SLSTR bands on top of a vegetation spectrum. OLCI bands are denoted with "Oa", SLSTR bands with "S". The SLSTR bands in the thermal infrared (S7, S8, S9, F1 and F2) are not shown.

2.3 Sentinel-2 surface reflectances

The Multi-spectral Instrument (MSI) onboard the Sentinel-2 satellites provides observations with 10 and 20 m spectral resolution. The use of older archived Sentinel-2 data at level 1 requires topographic and atmospheric correction and cloud detection in order to retrieve level 2 surface reflectances. The data will be corrected by using the algorithms in the FORCE software (Frantz, 2019). FORCE seem to better perform cloud detection than Sen2Cor and is therefore preferred over using the L2A product directly. Sentinel-2 data will be acquired for selected fire events in order to estimate the normalised burn ratio as a proxy for burned area and to quantify fire severity and combustion completeness from surface changes.

2.4 Sentinel-1 C-band backscatter

The Sentinel-1 C-band Synthetic Aperture Radar provides Radar backscatter. Backscatter observations allow to estimate surface soil moisture (Bauer-Marschallinger et al., 2019) and are also sensitive to LFMC (Wang et al., 2019; Rao et al., 2020). Hence Sentinel-1 backscatter will be used on an experimental case as proxy for fuel moisture content and hence to estimate combustion completeness.
For this purpose we plan to use the Sentinel-1 Global Backscatter Model (S1GBM)(https://sentinels.copernicus.eu/web/sentinel/missions/sentinel-1/sentinel-1-global-backscatter-model) as well as Sentinel-1 datasets in selected case studies.

2.5 Soil moisture_cci

The soil moisture_cci datasets combines various soil moisture retrievals from active and passive sensors in one harmonised long-term time series of soil moisture (Dorigo et al., 2017). The dataset is available at a spatial resolution of 0.25 x 0.25° for the period 1978-2020. The dataset will be explored as proxy to account for the effect of surface moisture on combustion completeness.

2.6 Metop-ASCAT

The soil water index from Metop/ASCAT is a proxy for soil moisture in various depths. The dataset is available at a resolution of 0.1° for the period since 2007 (Bauer-Marschallinger et al., 2018). The SWI will be used as proxy for surface fuel moisture content.

2.7 Biomass_cci

AGB from Biomass_cci is available at 100 m spatial resolution for the years 2010, 2017 and 2018 (Santoro et al., 2021). The dataset provides the total AGB of all woody components (stem, bark, branches, and twigs) of trees and comes with an estimate of uncertainty. The AGB maps from the different years should not be used to calculate any temporal changes in AGB. We will use the AGB from 2017 as input to our methodology to estimate fuel loads by providing a constraint on the total woody AGB.

2.8 Global Forest Canopy Height

The map of forest canopy height from Potapov et al. (2021) combines estimates of canopy height from the GEDI space-borne Lidar with observations from Landsat to produce a global map of forest canopy height at 30 m spatial resolution. The dataset is a major advancement over the long-lasting state-of-the-art dataset by Simard et al. (2011). We will use the GEDI/Landsat-based dataset as a constraint on tree height in order to estimate above-ground biomass in different tree compartments (stems, branches, leaves) in an allometry model.

2.9 Land cover_cci

Land cover maps from the CCI provide annual maps of the distribution of land cover classes for the years 1992 to 2015 at 300 m spatial resolution. This is completed by the C3S land cover maps for the years 2016 to 2020. The maps are developed in a way to be used for assessments of land cover change. Land cover maps provide information about the type of vegetation and hence the susceptibility of land to fire occurrence (Vilar et al., 2019). The maps will be used as input to estimate fuel loads by providing information on the fractional cover of herbaceous vegetation and trees and tree types. The maps will be also used to mask water bodies and wetlands.

2.10 Global fuelbed map

Global fuelbed map (Pettinari and Chuvieco, 2016) will be used as a constraint on surface fuels (litter, dead wood). These large scale gridded datasets on surface properties will be complemented by collections of in situ data to calibrate and evaluate methods.

2.11 North American Wildland Fuel database (NAWFD)

The NAWFD provides a map of existing vegetation types for the United States and for each vegetation type associated measurements and statistical distributions of fuel loads for different fuel types such as trees, shrubs, herbaceous vegetation, fine and coarse woody debris, litter and duff. (Prichard et al., 2019). The dataset will be used as reference to develop machine learning models to estimate surface fuels with associated uncertainties.

2.12 Biomass And Allometry Database (BAAD)

The BAAD provides field and greenhouse measurements of tree allometry (e.g. tree height, DBH) and biomass in tree components such as leaves, branches, and stems for various tree species and functional groups (Falster et al., 2015). This information will be used to calibrate allometric models between tree height, AGB and biomass in stems, branches and leaves in order to estimate fuel loads for different tree components.

2.13 VODCA VOD

The VODCA dataset provides harmonised time series of VOD in Ku-, X- and C-bands at 0.25° spatial resolution for the period 1987-2017, 1997-2018, and 2002-2018, respectively (Moesinger et al., 2020). Here, we will focus either on C-band or X-band. The dataset will be used to constrain parameters of our approach with respect to the temporal dynamics in fuel moisture and biomass at large scales.

2.14 SMOS VOD (LPRM)

Additionally, the usability of VOD in L-band from SMOS will be assessed. Several studies demonstrated the use of VOD from the SMOS-IC retrieval algorithm to estimate changes in AGB (Wigneron et al., 2021). However, here we will use VOD retrievals from SMOS obtained with the Land Parameter Retrieval Model (LPRM) algorithm (van der Schalie et al., 2017) to ensure consistency in the underlying radiative transfer with the VODCA dataset. The VOD datasets that are harmonised in VODCA were also retrieved with LPRM.

2.15 MODIS LFMC

Retrievals of LFMC from MODIS were recently developed for Australia (Yebra et al., 2018). The dataset provides 8-daily estimates of LFMC at 500 m resolution. The approach is also applied to estimate LFMC for California, South Africa, and Europe. The dataset will be used as benchmark for our own estimates of LFMC.

2.16 PRODES Historic deforestation rates

We will use several datasets to aid the identification of regional fire types. We will use estimates of historic deforestation from the PRODES dataset for Brazil to as one indicator to help separate deforestation from forest fires.

2.17 Hansen forest loss

Tree cover is an important ecological indicator of different fire types and dynamics. For example, a tree cover fraction of 50% can be used to separate tropical dry forests from more open savannah ecosystems relevant for our fire type classification. Patterns of tree cover loss following a fire can also help to further separate fire type and ecosystem impacts.

2.18 High latitude peatland extent and carbon

We will overlay our fire object database with a map of peatland extent and carbon storage (Hugelius et al., 2020). We will explore the use of a peatland map to identify peatland fires in high-latitude regions. Peatland fires are of particular concern because they are typically associated with long emissions lifetime, low combustion efficiency, and high methane emissions.

3 Individual fire behaviour

3.1 Sentinel-3 SLSTR active fire detections, FRP

The Sentinel-3 SLSTR instrument includes specific bands for fire detection and characterisation of Fire Radiative Power at 1 km spatial resolution at nadir. Active fire

detections will be used in our algorithm to identify fire location, type and quantify carbon emissions. The original algorithm to detect active fires with SLSTR was developed by Wooster et al. (2012), and then further improved by Xu et al., 2020. Data are operationally available through the Copernicus Open Access hub. Initial results highlight improved sensitivity compared to Terra-MODIS even at comparable view zenith angle (Xu et al., 2020). Combined, the S-3a and b provide global daily coverage in a 10 am / pm sun synchronous orbit.

3.2 NOAA20/S-NPP VIIRS active fire detections, FRP

The VIIRS instruments onboard NOAA20 and S-NPP provide relatively high resolution 375 m bands in the thermal domain resulting in unprecedented capability to detect low intensity fires. In addition, the onboard pixel aggregation scheme reduces the off-nadir increase in pixel size, and therefore minimum FRP detection threshold. The 375 m active fire product developed by Schroeder et al., 2014 is operationally available through NASA's FIRMS and from a NOAA FTP server. NOAA-20 and S-NPP are in the same sun synchronous 1:30 am / pm orbit, but spaced 50 minutes (half an orbit). As a result, the 3,000 km swaths of the instruments overlap and an area observed at near-nadir by one VIIRS instrument would be observed at off-nadir angles 50 minutes later by the other VIIRS instruments. The result is consistent near-nadir global coverage and slightly complementary timing of the overpass.

3.3 Sentinel-2 Fire cci burned area

Sentinel-2a and 2b provide an incredible potential to map global burned area at unprecedented resolution. In particular, the 5- day temporal resolution is critical in areas of frequent cloud cover near, near the end or beginning of the fire seasons. The 20-m spatial resolution enables disentangling of burned and unburned landscapes at very fine scale. Currently, Sentinel-2 burned area are available through FireCCI for 2016 and 2019 for Africa (Roteta et al., 2019). First results highlight about 80% more burned area than previously estimated using coarse resolution sensors (Ramo et al., 2021), mainly originating from small short-lived fires. In our study we will use these data to calibrate and validate burned area estimates associated with our active fire derived fire objects.

4 Atmospheric conditions and fire emissions

4.1 L2_CO (Sentinel-5p)

Carbon monoxide (CO) can either be produced by atmospheric oxidation of hydrocarbons, or during the combustion process, where is marks incomplete burning and thus provides a proxy for combustion efficiency. The hyperspectral Sentinel-5p satellite derives CO data from the shortwave infrared (SWIR) part of the solar spectrum (2305 nm

and 2385 nm) at 7×7 km spatial resolution (7×5.5 km from 6 August 2019 onwards). At these wavelengths, sensitivity to altitude – especially the troposphere – is approximately uniform, allowing TROPOMI to see all the way down to earth's surface. Combined with improved detector performance compared to its predecessor satellite like SCIAMACHY, this allows Sentinel-5p to observe fire emission plumes on a daily basis. Note that CO cannot be observed over oceans and snow/ice due to their low SWIR reflectance, unless there are clouds present (highly reflective at SWIR wavelengths).

4.2 L2_NO2 (Sentinel-5p)

Nitrogen dioxide (NO_2) is emitted by combustion processes, and emissions increase with increasing combustion temperature, thus providing a proxy for combustion efficiency. The hyperspectral Sentinel-5p satellite derives NO_2 data from visible wavelengths (405-465 nm) at 3.5×7 km spatial resolution (3.5×5.5 km from 6 August 2019 onwards). Tropospheric NO_2 columns are derived from total NO_2 columns by subtracting the (smooth) stratospheric NO_2 column which is based on global data assimilated total NO_2 columns. Combined with improved detector performance compared to its predecessor satellites like SCIAMACHY, OMI, and GOME-2, this allows Sentinel-5p to observe fire emission plumes on a once-daily basis. At higher latitudes ($\gtrsim 45°$) multiple overpasses per day can occur due to the Polar orbit of Sentinel-5p. At very high latitudes ($\gtrsim 60°$) during Polar summer daytime orbits crossing over the poles also remain sunlit that can result in even more overpasses. However, for those orbits the solar zenith angles become very large, reducing the accuracy and precision of the Sentinel-5p measurements. In practice, for the high latitude regions explored in Sense4Fire Sentinel-5p will deliver 2-3 consecutive useful orbits.

4.3 L2_HCHO (Sentinel-5p)

Formaldehyde (HCHO) is an intermediate gas in almost all oxidation chains of Non-Methane Volatile Organic Compounds (NMVOC), leading eventually to CO_2. The major HCHO source in the remote atmosphere is CH_4 oxidation. Over the continents, the oxidation of higher NMVOCs emitted from vegetation, fires, traffic and industrial sources results in important and localised enhancements of the HCHO levels. The hyperspectral Sentinel-5p satellite derives NO_2 data from visible wavelengths 326 and 360 nm at 3.5×7 km spatial resolution (3.5×5.5 km from 6 August 2019 onwards). Although Sentinel-5p measurements of HCHO are much better than those of its predecessor satellites SCIAMACHY, OMI, and GOME-2, they still require averaging over time (typically at 30 days or longer) to reduce measurement noise and uncover meaningful spatial patterns for comparison with similarly sampled average model simulation results.

4.4 L2_AER_AI (Sentinel-5p)

The Sentinel-5p absorbing aerosol index (AAI or UVAI) is a useful indicator for the presence of aerosols that absorb visible light (340 / 380 nm wavelength pair) at 3.5×7 km spatial resolution (3.5×5.5 km from 6 August 2019 onwards). The relatively simple calculation of the AAI is based on wavelength dependent changes in Rayleigh scattering in the UV spectral range where ozone absorption is very small. AAI can also be calculated in the presence of clouds so that daily, global coverage is possible. Due to calibration issues the Sentinel-5p AAI currently suffers from a cross-swath gradient bias, but nevertheless can be used for tracking the evolution of episodic aerosol plumes from dust outbreaks, volcanic ash, and biomass burning.

4.5 L2_AER_ALH (Sentinel-5p)

The TROPOMI Aerosol Layer Height product focuses on retrieval of vertically localised aerosol layers in the free troposphere, such as desert dust, biomass burning aerosol, or volcanic ash plumes. The height of such layers is retrieved for cloud-free conditions. Height information for aerosols in the free troposphere is particularly important for aviation safety. Aerosol height information also helps to interpret the UV Aerosol Index (UVAI) in terms of aerosol absorption as the index is strongly height-dependent. The current implementation of the algorithm is based on a neural network forward model and an optimal estimation scheme in the retrieval applied to oxygen absorption at the O2-A band (wavelengths ~758–770 nm). The main fit parameters are: aerosol layer mid pressure (pmid) and aerosol optical thickness (τ_0). The ALH data is available at 3.5×7 km spatial resolution (3.5×5.5 km from 6 August 2019 onwards). Note that currently the ALH is only retrieved for not optically very thick aerosol plumes (AOD < 5, see (Nanda et al., 2020)).

4.6 GFAS

The Global Fire Assimilation System (GFAS) is the standard fire emission product maintained and developed further as part of the Copernicus Atmosphere Monitoring Service (Kaiser et al., 2012). It calculates biomass burning emissions by assimilating Fire Radiative Power (FRP) observations from the MODIS instruments onboard the Terra and Aqua satellites and corrects for gaps in the observations, which are mostly due to cloud cover, and filters spurious FRP observations of volcanoes, gas flares and other industrial activity. The combustion rate is subsequently calculated with land cover-specific conversion factors, using a scaling based on GFED data. Land-use specific emission factors are adopted resulting in specific gas-phase and aerosol trace species emissions. The operational version with daily emission estimates is GFASv1.2, available on a 0.1° resolution, while also emission estimates from an updated version (GFASv1.4, including hourly emission estimates) are available.

4.7 GFED

The Global Fire Emissions Database (van der Werf et al., 2017) combines satellite information on fire activity and vegetation productivity to estimated gridded monthly burned area and fire emissions, as well as scalars that can be used to calculate higher temporal resolution emissions (sub-monthly and diurnal variations). Most of the resulting datasets are downloadable for use in large-scale atmospheric and biogeochemical studies. The core datasets are burned area, burned area from small fires based on active fire detections outside the burned area maps, carbon and dry matter emissions, fraction contributions of various fire types tot total emissions, and a list of emission factors to compute trace gas and aerosol emissions. missions data are available for carbon (C), dry matter (DM), carbon dioxide (CO_2), carbon monoxide (CO), methane (CH_4), hydrogen (H_2), nitrous oxide (N_2O), nitrogen oxides (NO_x), non-methane hydrocarbons (NMHC), organic carbon (OC), black carbon (BC), particulate matter 2.5 microns (PM2.5), total particulate matter (TPM), and sulphur dioxide (SO_2) among others. The current GFED version is v4 which has a spatial resolution of 0.25° and is available from 1997 onwards. The most recent year is 2016 but monthly emissions are available for the period after 2016 as yet-to-be consolidated (beta) data.

References

Bauer-Marschallinger, B., Paulik, C., Hochstöger, S., Mistelbauer, T., Modanesi, S., Ciabatta, L., Massari, C., Brocca, L., and Wagner, W.: Soil Moisture from Fusion of Scatterometer and SAR: Closing the Scale Gap with Temporal Filtering, Remote Sens., 10, 1030, https://doi.org/10.3390/rs10071030, 2018.

Bauer-Marschallinger, B., Freeman, V., Cao, S., Paulik, C., Schaufler, S., Stachl, T., Modanesi, S., Massari, C., Ciabatta, L., Brocca, L., and Wagner, W.: Toward Global Soil Moisture Monitoring With Sentinel-1: Harnessing Assets and Overcoming Obstacles, IEEE Trans. Geosci. Remote Sens., 57, 520–539, https://doi.org/10.1109/TGRS.2018.2858004, 2019.

Dorigo, W., Wagner, W., Albergel, C., Albrecht, F., Balsamo, G., Brocca, L., Chung, D., Ertl, M., Forkel, M., Gruber, A., Haas, E., Hamer, P. D., Hirschi, M., Ikonen, J., de Jeu, R., Kidd, R., Lahoz, W., Liu, Y. Y., Miralles, D., Mistelbauer, T., Nicolai-Shaw, N., Parinussa, R., Pratola, C., Reimer, C., van der Schalie, R., Seneviratne, S. I., Smolander, T., and Lecomte, P.: ESA CCI Soil Moisture for improved Earth system understanding: State-of-the art and future directions, Remote Sens. Environ., 203, 185–215, https://doi.org/10.1016/j.rse.2017.07.001, 2017.

Falster, D. S., Duursma, R. A., Ishihara, M. I., Barneche, D. R., FitzJohn, R. G., Vårhammar, A., Aiba, M., Ando, M., Anten, N., Aspinwall, M. J., Baltzer, J. L., Baraloto, C., Battaglia, M., Battles, J. J., Bond-Lamberty, B., van Breugel, M., Camac, J., Claveau, Y., Coll, L., Dannoura, M., Delagrange, S., Domec, J.-C., Fatemi, F., Feng, W., Gargaglione, V., Goto, Y., Hagihara, A., Hall, J. S., Hamilton, S., Harja, D., Hiura, T., Holdaway, R., Hutley, L. S., Ichie, T., Jokela, E. J., Kantola, A., Kelly, J. W. G., Kenzo, T., King, D., Kloeppel, B. D., Kohyama, T., Komiyama, A., Laclau, J.-P., Lusk, C. H., Maguire, D. A., le Maire, G., Mäkelä, A., Markesteijn, L., Marshall, J., McCulloh, K., Miyata, I., Mokany, K., Mori, S., Myster, R. W., Nagano, M., Naidu, S. L., Nouvellon, Y., O'Grady, A. P., O'Hara, K. L., Ohtsuka, T., Osada, N., Osunkoya, O. O., Peri, P. L., Petritan, A. M., Poorter, L., Portsmuth, A.,

Potvin, C., Ransijn, J., Reid, D., Ribeiro, S. C., Roberts, S. D., Rodríguez, R., Saldaña-Acosta, A., Santa-Regina, I., Sasa, K., Selaya, N. G., Sillett, S. C., Sterck, F., Takagi, K., Tange, T., Tanouchi, H., Tissue, D., Umehara, T., Utsugi, H., Vadeboncoeur, M. A., Valladares, F., Vanninen, P., Wang, J. R., Wenk, E., Williams, R., de Aquino Ximenes, F., Yamaba, A., Yamada, T., Yamakura, T., Yanai, R. D., and York, R. A.: BAAD: a Biomass And Allometry Database for woody plants, Ecology, 96, 1445–1445, https://doi.org/10.1890/14-1889.1, 2015.

Frantz, D.: FORCE—Landsat + Sentinel-2 Analysis Ready Data and Beyond, Remote Sens., 11, 1124, https://doi.org/10.3390/rs11091124, 2019.

Hansen, M. C., Potapov, P. V., Moore, R., Hancher, M., Turubanova, S. A., Tyukavina, A., Thau, D., Stehman, S., Goetz, S. J., Loveland, T. R., and others: High-resolution global maps of 21st-century forest cover change, science, 342, 850–853, 2013.

Hugelius, G., Loisel, J., Chadburn, S., Jackson, R. B., Jones, M., MacDonald, G., Marushchak, M., Olefeldt, D., Packalen, M., Siewert, M. B., and others: Large stocks of peatland carbon and nitrogen are vulnerable to permafrost thaw, Proc. Natl. Acad. Sci., 117, 20438–20446, 2020.

Kaiser, J. W., Heil, A., Andreae, M. O., Benedetti, A., Chubarova, N., Jones, L., Morcrette, J.-J., Razinger, M., Schultz, M. G., Suttie, M., and van der Werf, G. R.: Biomass burning emissions estimated with a global fire assimilation system based on observed fire radiative power, Biogeosciences, 9, 527–554, https://doi.org/10.5194/bg-9-527-2012, 2012.

Moesinger, L., Dorigo, W., Jeu, R. de, Schalie, R. van der, Scanlon, T., Teubner, I., and Forkel, M.: The global long-term microwave Vegetation Optical Depth Climate Archive (VODCA), Earth Syst. Sci. Data, 12, 177–196, https://doi.org/10.5194/essd-12-177-2020, 2020.

Nanda, S., Graaf, M. de, Veefkind, J. P., Sneep, M., Linden, M. ter, Sun, J., and Levelt, P. F.: A first comparison of TROPOMI aerosol layer height (ALH) to CALIOP data, Atmospheric Meas. Tech., 13, 3043–3059, 2020.

Pettinari, M. L. and Chuvieco, E.: Generation of a global fuel data set using the Fuel Characteristic Classification System, Biogeosciences, 13, 2061–2076, https://doi.org/10.5194/bg-13-2061-2016, 2016.

Potapov, P., Li, X., Hernandez-Serna, A., Tyukavina, A., Hansen, M. C., Kommareddy, A., Pickens, A., Turubanova, S., Tang, H., Silva, C. E., Armston, J., Dubayah, R., Blair, J. B., and Hofton, M.: Mapping global forest canopy height through integration of GEDI and Landsat data, Remote Sens. Environ., 253, 112165, https://doi.org/10.1016/j.rse.2020.112165, 2021.

Prichard, S. J., Kennedy, M. C., Andreu, A. G., Eagle, P. C., French, N. H., and Billmire, M.: Next-Generation Biomass Mapping for Regional Emissions and Carbon Inventories: Incorporating Uncertainty in Wildland Fuel Characterization, J. Geophys. Res. Biogeosciences, 124, 3699–3716, https://doi.org/10.1029/2019JG005083, 2019.

Ramo, R., Roteta, E., Bistinas, I., Wees, D. van, Bastarrika, A., Chuvieco, E., and Werf, G. R. van der: African burned area and fire carbon emissions are strongly impacted by small fires undetected by coarse resolution satellite data, Proc. Natl. Acad. Sci., 118, https://doi.org/10.1073/pnas.2011160118, 2021.

Rao, K., Williams, A. P., Flefil, J. F., and Konings, A. G.: SAR-enhanced mapping of live fuel moisture content, Remote Sens. Environ., 245, 111797, https://doi.org/10.1016/j.rse.2020.111797, 2020.

Roteta, E., Bastarrika, A., Padilla, M., Storm, T., and Chuvieco, E.: Development of a Sentinel-2 burned area algorithm: Generation of a small fire database for sub-Saharan Africa, Remote Sens. Environ., 222, 1–17, 2019.

Santoro, M., Cartus, O., Carvalhais, N., Rozendaal, D. M. A., Avitabile, V., Araza, A., de Bruin, S., Herold, M., Quegan, S., Rodríguez-Veiga, P., Balzter, H., Carreiras, J., Schepaschenko, D., Korets, M., Shimada, M., Itoh, T., Moreno Martínez, Á., Cavlovic, J., Cazzolla Gatti, R., da Conceição Bispo, P., Dewnath, N., Labrière, N., Liang, J., Lindsell, J., Mitchard, E. T. A., Morel, A., Pacheco Pascagaza, A. M., Ryan, C. M., Slik, F., Vaglio Laurin, G., Verbeeck, H., Wijaya, A., and Willcock, S.: The global forest above-ground biomass pool for 2010 estimated from high-resolution satellite observations, Earth Syst. Sci. Data, 13, 3927–3950, https://doi.org/10.5194/essd-13-3927-2021, 2021.

van der Schalie, R., de Jeu, R. A. M., Kerr, Y. H., Wigneron, J. P., Rodríguez-Fernández, N. J., Al-Yaari, A., Parinussa, R. M., Mecklenburg, S., and Drusch, M.: The merging of radiative transfer based surface soil moisture data from SMOS and AMSR-E, Remote Sens. Environ., 189, 180–193, https://doi.org/10.1016/j.rse.2016.11.026, 2017.

Schroeder, W., Oliva, P., Giglio, L., and Csiszar, I. A.: The New VIIRS 375 m active fire detection data product: Algorithm description and initial assessment, Remote Sens. Environ., 143, 85–96, 2014.

Simard, M., Pinto, N., Fisher, J. B., and Baccini, A.: Mapping forest canopy height globally with spaceborne lidar, J. Geophys. Res. Biogeosciences, 116, G04021, https://doi.org/10.1029/2011JG001708, 2011.

Vilar, L., Garrido, J., Echavarría, P., Martínez-Vega, J., and Martín, M. P.: Comparative analysis of CORINE and climate change initiative land cover maps in Europe: Implications for wildfire occurrence estimation at regional and local scales, Int. J. Appl. Earth Obs. Geoinformation, 78, 102–117, https://doi.org/10.1016/j.jag.2019.01.019, 2019.

Wang, L., Quan, X., He, B., Yebra, M., Xing, M., and Liu, X.: Assessment of the Dual Polarimetric Sentinel-1A Data for Forest Fuel Moisture Content Estimation, Remote Sens., 11, 1568, https://doi.org/10.3390/rs11131568, 2019.

Weidong, X., Wooster, M. J., He, J., and Zhang, T.: First study of Sentinel-3 SLSTR active fire detection and FRP retrieval: Night-time algorithm enhancements and global intercomparison to MODIS and VIIRS AF products, Remote Sens. Environ., 248, 111947, 2020.

van der Werf, G. R., Randerson, J. T., Giglio, L., Van Leeuwen, T. T., Chen, Y., Rogers, B. M., Mu, M., Van Marle, M. J., Morton, D. C., Collatz, G. J., and others: Global fire emissions estimates during 1997-2016, Earth Syst. Sci. Data, 9, 697–720, 2017.

Wigneron, J.-P., Li, X., Frappart, F., Fan, L., Al-Yaari, A., De Lannoy, G., Liu, X., Wang, M., Le Masson, E., and Moisy, C.: SMOS-IC data record of soil moisture and L-VOD: Historical development, applications and perspectives, Remote Sens. Environ., 254, 112238, https://doi.org/10.1016/j.rse.2020.112238, 2021.

Wooster, M. J., Xu, W., and Nightingale, T.: Sentinel-3 SLSTR active fire detection and FRP product: Pre-launch algorithm development and performance evaluation using MODIS and ASTER datasets, Remote Sens. Environ., 120, 236–254, https://doi.org/10.1016/j.rse.2011.09.033, 2012.

Xu, W., Wooster, M. J., He, J., and Zhang, T.: First study of Sentinel-3 SLSTR active fire detection and FRP retrieval: Night-time algorithm enhancements and global intercomparison to MODIS and VIIRS AF products, Remote Sens. Environ., 248, 111947, https://doi.org/10.1016/j.rse.2020.111947, 2020.

Yebra, M., Quan, X., Riaño, D., Rozas Larraondo, P., van Dijk, A. I. J. M., and Cary, G. J.: A fuel moisture content and flammability monitoring methodology for continental Australia based on optical

remote sensing, Remote Sens. Environ., 212, 260–272, https://doi.org/10.1016/j.rse.2018.04.053, 2018.

Yebra, M., Scortechini, G., Badi, A., Beget, M. E., Boer, M. M., Bradstock, R., Chuvieco, E., Danson, F. M., Dennison, P., Dios, V. R. de, Bella, C. M. D., Forsyth, G., Frost, P., Garcia, M., Hamdi, A., He, B., Jolly, M., Kraaij, T., Martín, M. P., Mouillot, F., Newnham, G., Nolan, R. H., Pellizzaro, G., Qi, Y., Quan, X., Riaño, D., Roberts, D., Sow, M., and Ustin, S.: Globe-LFMC, a global plant water status database for vegetation ecophysiology and wildfire applications, Sci. Data, 6, 1–8, https://doi.org/10.1038/s41597-019-0164-9, 2019.